Electronic Supplementary Material (ESI) for Journal of Materials Chemistry C.

Supporting Information

Direct Z-scheme Sn-In_2O_3/In_2S_3 heterojunction nanostructures for enhanced photocatalytic CO_2 reduction activity

Yinyi Ma[a], Zemin Zhang[a], Xiao Jiang[a], Rongke Sun[a], Mingzheng Xie[b], and Weihua Han[*a]

[a] *School of Physical Science and Technology, Lanzhou University, Lanzhou 730000, China.*

[b] *College of Earth and Environmental Sciences, Lanzhou University, Lanzhou 730000, China.*

E-mail: hanwh@lzu.edu.cn (Weihua Han)

Equations used in this work

The conversion between potentials vs. Ag/AgCl and those vs. RHE is performed using the equation below:

$$E\ (vs.\ \text{RHE}) = E\ (vs.\ \text{Ag/AgCl}) + E^{o}_{\text{Ag/AgCl}} + 0.0591\ \text{V} \times \text{pH}$$

$$E\ (vs.\ \text{NHE}) = E\ (vs.\ \text{Ag/AgCl}) + E^{o}_{\text{Ag/AgCl}}$$

($E^{o}_{\text{Ag/AgCl}}$ =0.1976 V *vs*. NHE at 25 °C)

1. Kubelka-Munk function

The Kubelka-Munk function can be described as following equation (1):

$$(F(R_\infty)h\nu)^{n} = A\ (h\nu - E_g) \quad (1)$$

$$F(R_\infty) = \frac{(1 - R\infty)^2}{2R\infty} \quad (2)$$

$$R_\infty = \frac{Rsample}{Rstandard} \quad (3)$$

where R_∞ is the reflectance of an infinitely thick specimen; $R_{standard}$ is the reflectance of $BaSO_4$; R_{sample} is the reflectance of catalyst; $h\nu$ is the incident photo's energy, E_g is the band gap, A is a constant of the material. The value of n is 2 because they are all direct band gap materials of In_2O_3 and In_2S_3.

2. Applied bias photon-to-current efficiency (ABPE)

ABPE was calculated according to eqn (4):

$$ABPE = \left[\frac{j(mA\ /\ cm^2) \times (1.23\ V - V_b)}{P_{total}(mW\ /\ cm^2)}\right]_{AM\ 1.5\ G} \quad (4)$$

where j is the photocurrent density obtained under an applied bias V_b, and P_{total} is the incident light intensity (100 mW/cm^2).[1]

3. Incident photon-to-current efficiency (IPCE)

IPCE measurements were made in a three-electrode setup with Ag/AgCl electrode and Pt counter electrode at 0.5 V (*vs.* Ag/AgCl). IPCE was calculated according to equation (5):

$$IPCE(\lambda) = \frac{\left| j_{ph}\left(mA/cm^2\right)\right| \times 1239.8(V \times nm)}{P_{mono}\left(mW/cm^2\right) \times \lambda(nm)} \quad (5)$$

where 1239.8 V × nm represents a multiplication of h (Planck's constant) and c (the speed of light), P_{mono} is the calibrated and monochromated illumination power intensity in mW/cm^2, and λ (nm) is the wavelength at which this illumination power is measured.[1]

4. Light harvesting efficiency (LHE)

LHE can be expressed as equation (6):

$$LHE = 1\text{-}10^{-A(\lambda)} \quad (6)$$

where A (λ) is absorbance, λ is wavelength.[2]

5. Absorbed photon to current efficiency (APCE)

By combining the equations for determining IPCE and $\eta_{e\text{-}/h+}$ experimentally, we can derive APCE as following equation (7):[2]

$$APCE(\lambda) = \frac{IPCE(\lambda)}{LHE} = \frac{\left| j_{ph}\left(mA/cm^2\right)\right| \times 1239.8(V \times nm)}{P_{mono}\left(mW/cm^2\right) \times \lambda(nm) \times (1 - 10^{-A(\lambda)})} \quad (7)$$

6. The flat band potential (E_{fb})

The flat band potential of the semiconductors was calculated by the Mott-Schottky relation (8):

$$\frac{1}{C^2} = \frac{2}{e_0 \varepsilon_0 \varepsilon_r N_d} \times \left(- E + E_{fb} - \frac{kT}{e} \right) \quad (8)$$

Where C is the capacitance of the electrode, e_0 is the elemental charge (1.6×10^{-19} C), ε_0 is the permittivity of vacuum (8.85×10^{-12} Fm^{-1}), ε_r is the dielectric constant of the semiconductor, E is the applied potential, k is Boltzmann constant ($1.38 \times 10{-}23$ J K^{-1}) and T is the temperature. E_{fb} is the potential of flat band, which can be obtained by extrapolating the linear region in the M-S diagram. At room temperature, kT/e is negligible. So the results shows that when $1/C^2$ is zero, the X-intercept is equal to the flat band potential (E_{fb}).

7. The charge separation efficiency and transfer efficiency

The charge separation efficiency (η_{sep}) is the fraction of the photo-generated holes that reach the surface, whereas the rest of the holes recombine with electrons within the photoanode before reaching the surface (bulk recombination). The charge transfer efficiency (η_{trans}), also called the injection efficiency, is the fraction of the holes that give rise to electrochemical reactions out of the holes that have reached the surface. The rest of the holes recombine with conduction band electrons at the surface (surface recombination).

The water splitting photocurrent (J_{H2O}) is a product of the rate of photon absorption expressed as a current density (J_{abs}), the charge separation efficiency of the photo generated carriers (η_{sep}), and charge transfer efficiency to the electrolyte (η_{trans}):

$$J_{H2O} = J_{abs} \times \eta_{sep} \times \eta_{trans} \quad (9)$$

η_{sep} is the fraction of photogenerated holes that does not recombine with electrons in the bulk. η_{trans} is the efficiency of those holes that have reached the electrode/electrolyte

interface and that are injected into the electrolyte to oxidize water, or in other words, do not recombine with electrons at surface traps. On the other hand, the photocurrent measured with Na_2SO_3 in the electrolyte (J_{Na2SO3}) is a product of J_{H2O} and η_{sep} only:

$$J_{Na2SO3} = J_{abs} \times \eta_{sep} \quad (10)$$

because the charge transfer efficiency becomes 100% ($\eta_{trans} = 1$) in the presence of the hole scavenger (Na_2SO_3) in the electrolyte. Because the light penetration depth in a semiconductor is wavelength-dependent, η_{sep} is sensitive to the spectral distribution of the incident light.[3, 4]

The charge transfer efficiency into water is achieved by dividing J_{H2O} by J_{Na2SO3}. By measuring the light absorption of the photoelectrode and integrating it with respect to the AM 1.5 G solar spectrum, J_{abs} was calculated to be 13.8 $mA \cdot cm^{-2}$ for the Sn-In_2O_3/In_2S_3 sample .With the charge transfer efficiency and J_{abs} both known, the charge separation efficiency was calculated by dividing J_{Na2SO3} by J_{abs}.

Supplementary figures

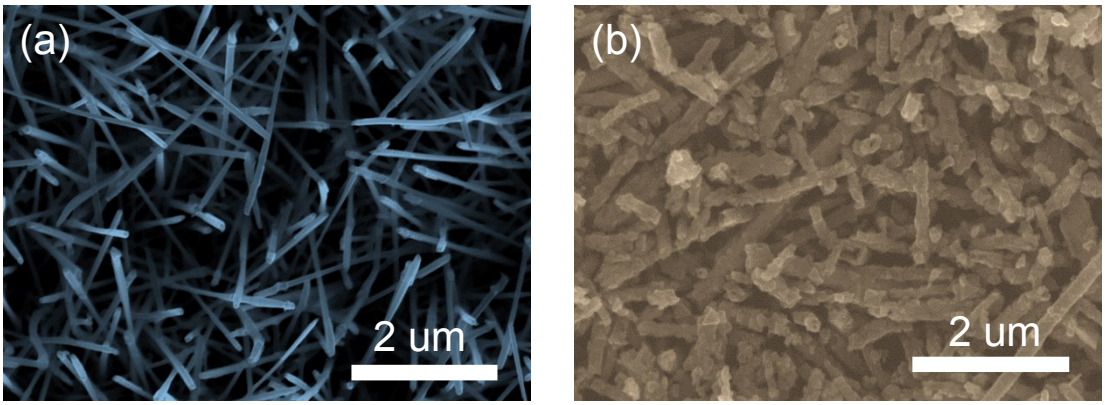

Figure S1. SEM image at low magnification of (a) Sn-In_2O_3 and (b) Sn-In_2O_3/ In_2S_3.

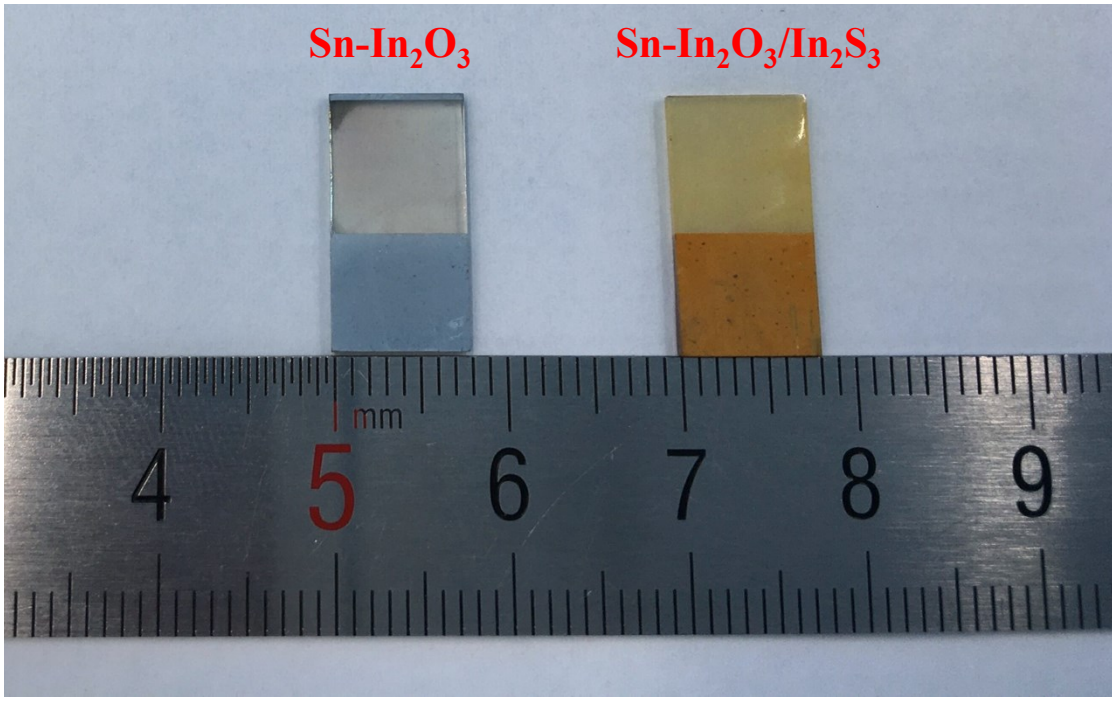

Figure S2. Photographs of Sn-In_2O_3 and Sn-In_2O_3/In_2S_3 .

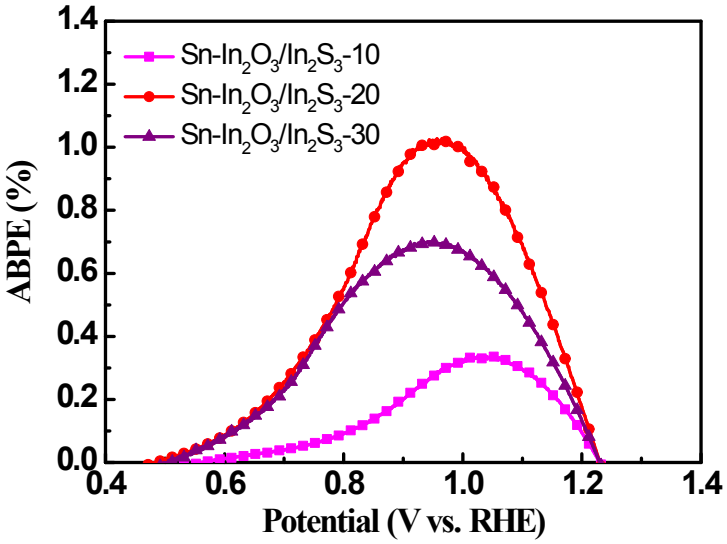

Figure S3. The ABPE graphs of samples with different sulfuration time.

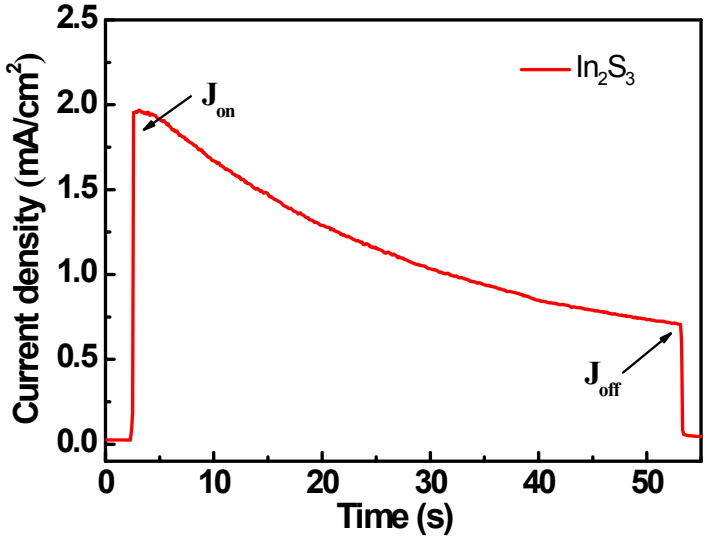

Figure S4. Stability test of In_2S_3 sample under simulated sunlight. The bias potential is 0.5 V (*vs*. Ag / AgCl).

Due to the strong photo-corrosion effect, the photocurrent of the bare In_2S_3 photoelectrode is rapidly reduced to a negligible level under 50 seconds of light irradiation.

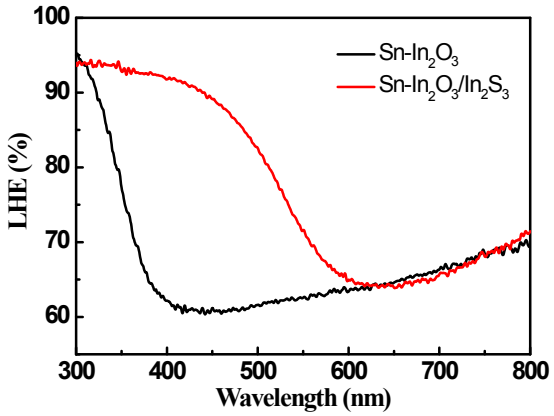

Figure S5. Light harvesting efficiency plot of different samples.

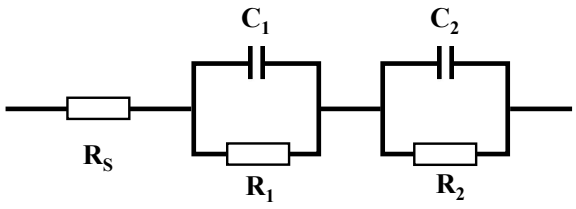

Figure S6. RC circuit model for Nyquist plot.

Rs is the series resistance of the entire electrochemical system. The first stage RC circuit (R_1 , C_1) is regarded as the charge transfer resistance and the capacitance of the semiconductor layer. R2 is the reaction impedance of the semiconductor/electrolyte interface.

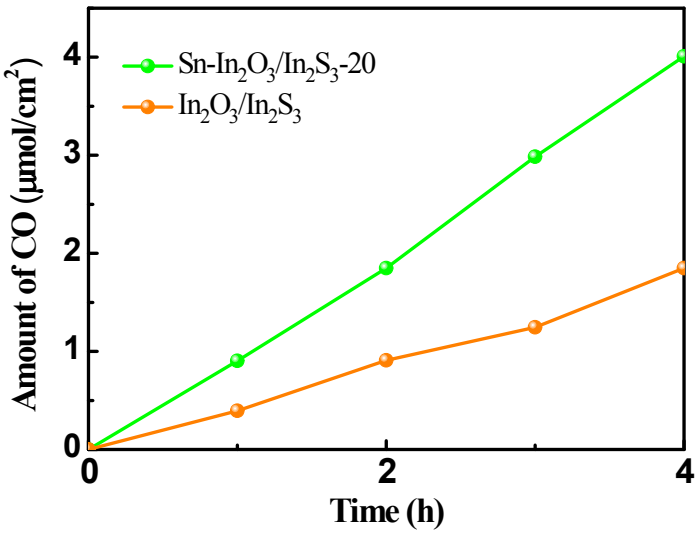

Figure S7. Photocatalytic CO_2 conversion under irradiation of light with wavelength longer than 420 nm.

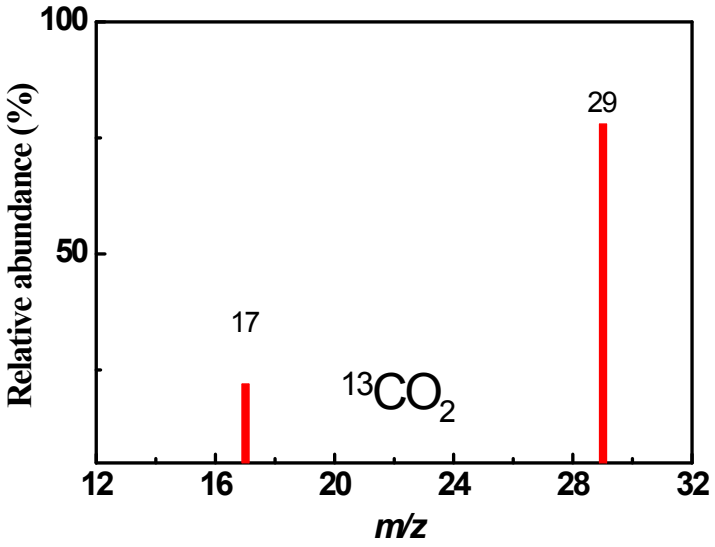

Figure S8. GC–MS data for the CO and CH_4 produced during photocatalytic reduction of $^{13}CO_2$ over SIOS-20 sample. m/z represents the mass/charge ratio of ions. The m/z at 17 and 29 are due to ^{13}CO and $^{13}CH_4$.

The isotope tracer experiment for the photoreduction of $^{13}CO_2$ (purity 99%) was carried out and

tested by gas chromatography - mass spectrometer (GC - MS) to determine the real source of the photocatalytic products.

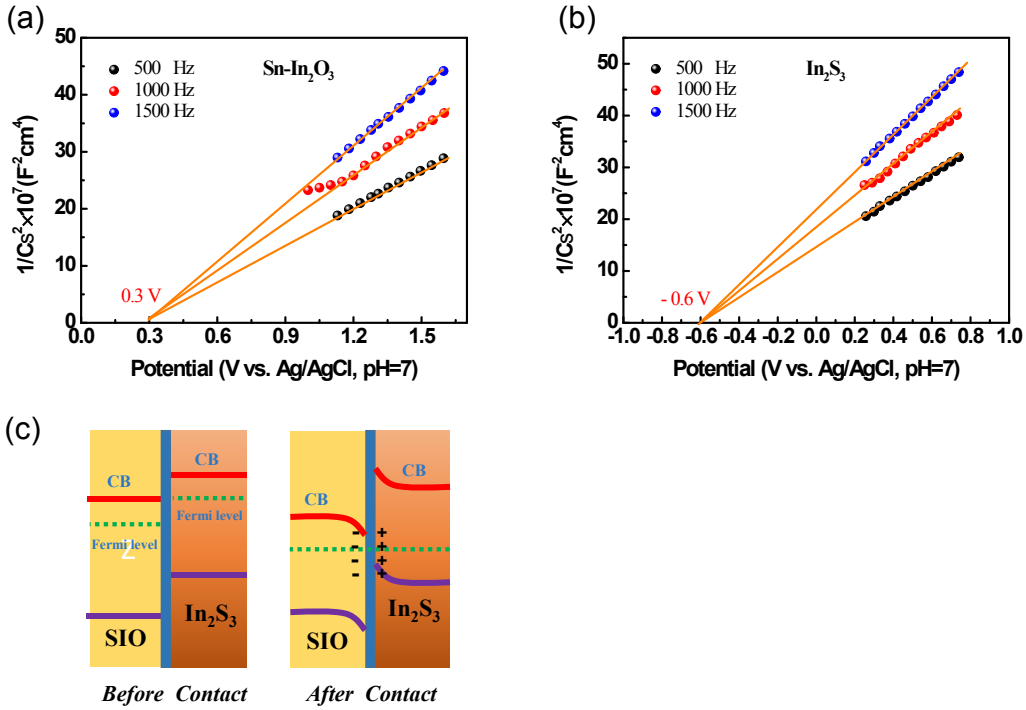

Figure S9. Mott-Schottky diagrams of pure Sn-In_2O_3 (a) and pure In_2S_3 (b) samples at different frequencies. The charge transfer mechanism at the interface (c).

The Mott-Schottky plots was measured in the dark state to evaluate the energy band structure of the prepared samples. As shown in Figure S9a and Figure S9b, the positive slope of the plot indicates the N-type nature of Sn-In_2O_3 and In_2S_3. By extrapolating the linear part of the M-S plot, the flat band potential (E_{fb}) of SIO and In_2S_3 are about 0.5 V and - 0.4 V (*vs.* NHE at pH=7), respectively. In a specific electrolyte, the E_{fb} reflects the location of the material's Fermi level (E_f)[5]. For N-type semiconductors, the energy difference between the bottom of the conduction band and the E_f is 0.2 eV. Considering the optical band gap of the samples, the energy band structure of the samples can be represented by Figure S9c. Usually, when the two

different semiconductors are brought together, due to the balance of the Fermi level, electrons will flow from the semiconductor with the high Fermi level to the semiconductor with the low Fermi level until they are aligned at the same level. Since the Fermi level of In_2S_3 is more negative than the Fermi level of SIO, this indicates that the electron will be transferred from In_2S_3 to SIO before reaching equilibrium. This creates a space charge region and a built-in electric field pointing from In_2S_3 (+) to SIO (-), which drives band bending at the interface. The directional built-in electric field and the interface band bending will facilitate the Z-scheme charge transfer mechanism at the SIO / In_2S_3 interface[6].

Table S1 The comparison of our work and other researches

Sample	Light source	CO yield rate ($\mu mol \cdot g^{-1} \cdot h^{-1}$)	CH_4 yield rate ($\mu mol \cdot g^{-1} \cdot h^{-1}$)	Reference
In_2O_3/TiO_2	500 W Hg lamp	39.5	124.5	7
In_2O_3/CeO_2/HATP	300 W Xe lamp	5.34	2.83	8
$ZnFe_2O_4$/RGO/In_2O_3	300 W Xe lamp	8.85	1.95	9
ZnO/g-C_3N_4	500 W Xe lamp (λ>420nm)	29	4	10
BiFeWOx/In_2S_3	300 W Xe lamp	28.9	49.9	11
WO_3/Au/In_2S_3	300 W Xe lamp ($\lambda > 420$ nm)	None	0.42	12
In_2S_3-$CdIn_2S_4$	300 W Xe lamp	825	None	13
(Au,C_3N_4)/TiO_2	300 W Xe lamp	193.2	44.8	14
$ZnIn_2S_4$	300 W Xe lamp	33.2	None	15
MOF (PCN-601)	300 W Xe lamp ($\lambda > 410$ nm)	6.0	10.1	16
	AM 1.5G	3.2	92	
Sn-In_2O_3/In_2S_3	**300 W Xe lamp**	**367.8**	**146**	**Our work**

References

1. Z. Chen, T. F. Jaramillo, T. G. Deutsch, A. Kleiman-Shwarsctein, A. J. Forman, N. Gaillard, R. Garland, K. Takanabe, C. Heske and M. Sunkara, *J. Mater. Res.*, 2010, **25**, 3-16.
2. K.-H. Ye, Z. Wang, J. Gu, S. Xiao, Y. Yuan, Y. Zhu, Y. Zhang, W. Mai and S. Yang, *Energy & Environmental Science*, 2017, **10**, 772-779.
3. H. Dotan, K. Sivula, M. Grätzel, A. Rothschild and S. C. Warren, *Energy & Environmental Science*, 2011, **4**, 958-964.
4. D. Klotz, D. A. Grave and A. Rothschild, *Phys. Chem. Chem. Phys.*, 2017, **19**, 20383-20392.
5. Q. Shi, Z. Li, L. Chen, X. Zhang, W. Han, M. Xie, J. Yang and L. Jing, *Appl. Catal., B*, 2019, **244**, 641-649.
6. Z.-F. Huang, J. Song, X. Wang, L. Pan, K. Li, X. Zhang, L. Wang and J.-J. Zou, *Nano Energy*, 2017, **40**, 308-316.
7. M. Tahir, B. Tahir, N. A. Saidina Amin and H. Alias, *Appl. Surf. Sci.*, 2016, **389**, 46-55.
8. J. Guan, H. Wang, J. Li, C. Ma and P. Huo, *J. Taiwan Inst. Chem. Eng.*, 2019, **99**, 93-103.
9. J. Li, F. Wei, C. Dong, W. Mu and X. Han, *J. Mater. Chem. A*, 2020, **8**, 6524-6531.
10. W. Yu, D. Xu and T. Peng, *Journal of Materials Chemistry A*, 2015, **3**, 19936-19947.
11. Y. Wang, Y. Zeng, S. Wan, S. Zhang and Q. Zhong, *J. CO2 Util.*, 2019, **29**, 156-162.
12. H. Li, Y. Gao, Y. Zhou, F. Fan, Q. Han, Q. Xu, X. Wang, M. Xiao, C. Li and Z. Zou, *Nano Lett.*, 2016, **16**, 5547-5552.
13. S. Wang, B. Y. Guan, Y. Lu and X. W. D. Lou, *J. Am. Chem. Soc.*, 2017, **139**, 17305-17308.
14. R. Sun, X. Jiang, M. Zhang, Y. Ma, X. Jiang, Z. Liu, Y. Wang, J. Yang, M. Xie and W. Han, *J. Catal.*, 2019, **378**, 192-200.
15. X. Jiao, Z. Chen, X. Li, Y. Sun, S. Gao, W. Yan, C. Wang, Q. Zhang, Y. Lin, Y. Luo and Y. Xie, *J. Am. Chem. Soc.*, 2017, **139**, 7586-7594.
16. Z.-B. Fang, T.-T. Liu, J. Liu, S. Jin, X.-P. Wu, X.-Q. Gong, K. Wang, Q. Yin, T.-F. Liu, R. Cao and H.-C. Zhou, *J. Am. Chem. Soc.*, 2020, **142**, 12515-12523.